Journal of Chromatography, 455 (1988) 1–15
Elsevier Science Publishers B.V., Amsterdam — Printed in The Netherlands

CHROM. 20 904

RESOLUTION OF COLLOIDAL LATEX AGGREGATES BY SEDIMENTATION FIELD-FLOW FRACTIONATION

HARLAN K. JONES*, BHAJENDRA N. BARMAN and J. CALVIN GIDDINGS*
Department of Chemistry, Henry Eyring Building, University of Utah, Salt Lake City, UT 84112 (U.S.A.)
(First received June 10th, 1988; revised manuscript received August 18th, 1988)

SUMMARY

The observation of a repetitive series of peaks while analyzing two different samples of poly(methyl methacrylate) colloidal latex spheres by sedimentation field-flow fractionation strongly suggests that part of the latex population has aggregated into doublets, triplets, and higher-order particle clusters. The aggregation hypothesis is confirmed for the two samples both by retention calculations and by electron microscopy. It is shown that the resolution of the latex clusters is influenced by flow velocity in a manner predicted by theory but that such resolution is limited by the polydispersities of the two latex samples. Polydispersity values are obtained using plate height *versus* flow velocity measurements and are shown to be consistent with the different resolution levels observed for the two colloids. A detailed analysis of the results shows that steric effects play an increasing role as cluster size increases. The steric role in this study is examined at some length.

INTRODUCTION

The separation of the components of complex colloidal materials is one of the most difficult challenges in separation science. Most chromatographic methods fail in the colloidal size range or, if operable, they perform poorly in terms of resolution, recovery, and reproducibility. Therefore it is desirable to examine alternate means that might solve important colloid separation and characterization problems encountered in working with biological, industrial, environmental, and geological materials.

The techniques of field-flow fractionation (FFF) appear to be well-suited to colloid analysis. The special subtechnique of sedimentation FFF is particularly effective in dealing with colloidal particles in the diameter range from 0.02 to 1 μm (up to 100 μm using the steric mode of operation). Not only is resolution high with the sedimentation subtechnique of FFF but separation occurs on the basis of differences in effective mass according to well-defined theoretical principles. The theoretical equations make it possible to calculate the properties of colloidal particles in terms of the elution characteristics observed for the particles in sedimentation FFF[1–3].

* Present address: Battelle PNL, Richland, WA 99352, U.S.A.

0021-9673/88/$03.50

One of the most important colloidal processes, and one that is generally quite difficult to characterize, is the aggregation of single particles to form complexes made up of multiples of the individual particles. Aggregation is a common phenomenon for both natural and industrial colloids[4,5]. However, the resolving power of sedimentation FFF has not been fully focussed on the separation and characterization of colloidal aggregates. The clearest demonstration of the ability of sedimentation FFF to separate aggregated colloids was reported from this laboratory in 1980[6]: a complex biomaterial sample was shown to emerge as singlet, doublet, and higher-order aggregated viral rods.

Because of their uniformity, samples of latex microspheres appear to provide an ideal medium for the study of aggregation. However, these samples generally consist only of single particles; when aggregation is forced (*e.g.*, by freezing or adding salt), the single particles will generally clump together out-of-control, forming an unmanageable precipitate. Thus in our extensive studies with polystyrene latex standards we have not until recently observed simple aggregates consisting of two, three, or more particles. However, in some recent studies undertaken to characterize poly(methyl methacrylate) (PMMA) latex samples using sedimentation FFF, we immediately observed a series of peaks (see Fig. 1) suggestive of low order aggregation. In pursuing these studies we have found that sedimentation FFF provides extraordinary detail on both the aggregates and the aggregation process. While some of the details of these studies will be reported in the colloid literature, we will examine here the characteristics of sedimentation FFF that must be considered for the resolution of aggregated materials.

Normal sedimentation FFF obeys the basic principles originally formulated by Giddings *et al.*[7]; the favorable agreement between theory and experiment has been demonstrated many times for latex particles up to 1 μm diameter[1,3,7–11]. When the effective particle size exceeds *ca.* 1 μm (specifically when the particle radius becomes larger than the mean thickness of the steady-state particle layer), the steric limit of FFF is approached[12]. Unlike normal FFF where smaller particles elute before larger ones, steric FFF has an elution order similar to hydrodynamic chromatography[13] with larger particles eluting first. However, some steric effects become evident before this inversion in elution order occurs.

This study focuses on the ability of sedimentation FFF to resolve aggregated species, specifically singlet, doublet, and higher order PMMA aggregates. Electron microscopy is used in conjunction with this work to confirm the presence of separated aggregate species.

THEORY

The basic retention equation for normal FFF operation is given by[1–3,7]

$$R = 6\lambda[\coth(1/2\lambda) - 2\lambda] \tag{1}$$

where R is the retention ratio and λ is the dimensionless FFF retention parameter, a measure of the compression of the particle distribution against the channel wall by the field. If the sample is highly retained, in which case R and λ are small, R can be approximated by the simple form

$$R = 6\lambda \quad (\lambda \to 0) \tag{2}$$

In sedimentation FFF, the retention parameter λ is related to particle mass m by the expression

$$\lambda = \frac{kT}{mwG\Delta\rho/\rho_s} \tag{3}$$

where k is the Boltzmann constant, T is the absolute temperature of the carrier liquid, G is the centrifugal acceleration, w is the channel thickness, $\Delta\rho$ is the difference in density between the particle and carrier liquid, and ρ_s is the density of the sample particles. If the particles are spherical in shape, the retention parameter λ can be rewritten in terms of the particle diameter d

$$\lambda = \frac{6kT}{\pi\Delta\rho wGd^3} \tag{4}$$

From the experimental retention volume V_R, the retention ratio R is obtained by using

$$R = V_0/V_R \tag{5}$$

where V_0 is the retention volume of nonretained material, equal to the channel void volume. The measured value of R is then used either to calculate particle mass from eqns. 1 and 3 or particle diameter (in the case of spherical particles) from eqns. 1 and 4.

The transition from normal sedimentation FFF to steric FFF has been predicted by theory[14] and demonstrated by experiment[15]. However, an exact theory for particle retention in the steric FFF region has yet to be developed. Steric FFF can be thought of as the high-field large-particle limit of normal FFF. In steric FFF differences in particle size control the differential migration of the particles[12].

The retention equation when modified for the steric FFF mechanism takes the following form[14,16]

$$R = \frac{3\gamma d}{w} + 6\lambda \tag{6}$$

where γ is a dimensionless factor of order unity. The factor γ has been shown to be influenced by several experimental parameters such as flow-rate, field strength, and particle density[14,15].

The resolution R_s between two neighboring component peaks in FFF is defined in the same way as in chromatography

$$R_s = \frac{\Delta z}{4\sigma} \tag{7}$$

where Δz is the distance between the centers of gravity of the two peaks and σ is the average standard deviation of the peaks. Resolution can be related to the apparent number of theoretical plates N and the retention ratio R in the following way[17]

$$R_s = \frac{N^{1/2}}{4} \frac{\Delta R}{R} \tag{8}$$

where ΔR is the difference in the retention ratio of the two peaks. If the sample is well retained ($R < 0.5$ as $\lambda < 0.1$) then R is approximately inversely proportional to particle mass as shown by combining eqns. 2 and 3. For small $\Delta R/R$ values eqn. 8 can be expressed as

$$R_s = \frac{N^{1/2}}{4} \frac{\Delta m}{m} \tag{9}$$

where Δm is the mass difference between the particles in the two neighboring peaks and m is the mean particle mass.

When FFF is applied to particles distributed over a small but finite diameter range, the high selectivity of FFF causes the fractionation of the particles according to size and consequently increases the width of the particle peak. The plate height contribution of this "polydispersity" effect is designated as H_p. The apparent plate height H of the system can be approximated as the sum of H_p and the non-equilibrium term $C<v>$

$$H = H_p + C<v> \tag{10}$$

where $<v>$ is the mean linear flow velocity and C is a constant independent of $<v>$. Since $N = L/H$, where L is channel length, eqn. 9 becomes

$$R_s = \frac{1}{4} \left(\frac{L}{H_p + C<v>} \right)^{1/2} \frac{\Delta m}{m} \tag{11}$$

which shows that for finite polydispersity the value of R_s cannot be reduced below a fixed minimum level no matter how small the "true" system plate height $C<v>$. However, if H_p is negligible, R_s will vary inversely as $<v>^{1/2}$.

Particle size polydispersity is expressed here by the coefficient of variation, equal to the ratio of the standard deviation σ_d in particle size to the mean particle diameter d. The coefficient of variation of single (non-aggregated) latex particles can be determined by plotting the sedimentation FFF plate height for the first (singlet) peak *versus* the linear flow velocity $<v>$ of the carrier liquid. As shown by eqn. 10, the intercept of such a plot can be equated to the polydispersity contribution to plate height, H_p. The latter is related to σ_d/d by[7]

$$H_p = 9LS^2(\sigma_d/d)^2 \tag{12}$$

where S is the mass selectivity (which approaches unity for highly retained particles in sedimentation FFF[18]) and L is the length of the FFF channel.

EXPERIMENTAL

Two sedimentation FFF systems were used in this work. The basic apparatus for system I is a slightly modified version of the Model S101 sedimentation FFF instrument from FFFractionation (Salt Lake City, UT, U.S.A.). The apparatus was employed with a channel having tip-to-tip length $L = 94.2$ cm, thickness $w = 0.0254$ cm, and breadth $b = 1.40$ cm. The channel void volume V_0 measured as the elution volume (minus extrachannel volume) of a non-retained sodium benzoate peak was found to be 3.25 ml (slightly reduced from the normal 4.5 ml volume of the Model S101 system), a value used for all experimental retention ratio calculations. The accumulation (outer) wall was coated with a polyimide tape for inertness. The distance r_0 between the channel and axis of rotation is 15.5 cm.

The system II sedimentation FFF apparatus is similar to that reported in an earlier paper[19]. The apparatus has provisions for stream-splitting at the outlet end of the channel to enhance detector signal[20]. The channel dimensions are 90.5 cm length, 2.0 cm breadth, and 0.0254 cm thickness. The void volume is 4.5 ml. The channel is secured inside an aluminum rotor with a radius r_0 of 15.3 cm. The system accumulation wall has a highly polished Hastelloy C surface.

The flow stream for both systems was delivered by Gilson Minipuls 2 peristaltic pumps (Middleton, WI, U.S.A.). All experiments were carried out at a constant field strength of 61.6 g (600 rpm) for system II and 111.0 g (800 rpm) for system I. Altex Model 153 UV detectors from Beckman Instruments (Berkeley, CA, U.S.A.) filtered at 254 nm wavelength were used. The detector response was transcribed onto Houston Instrument strip chart recorders (Austin, TX, U.S.A.).

The standard carrier liquid was deionized, distilled water which was further purified by a Sybron/Barnstead Nanopure filtration system (Boston, MA, U.S.A.). For system II, 0.05% by wt. sodium dodecyl sulfate and 0.01% by wt. sodium azide, both from Sigma (St. Louis, MO, U.S.A.), were added to water. However, for system I a solution of 0.1% by vol. FL-70 detergent (Fisher Scientific, Pittsburgh, PA, U.S.A.) and 0.02% by wt. sodium azide was used.

Two PMMA latex samples were used in this work. One sample was supplied by Dr. T. Provder of The Glidden Company (Strongsville, OH, U.S.A.). The particle diameter of the latex spheres in this sample was given as 0.207 μm and the density as 1.214 g/ml. A second PMMA sample obtained from Seradyn (Indianapolis, IN, U.S.A.) was reported to have a single particle diameter of 0.230 μm and a particle density of 1.21 g/ml.

Concurrent with the sedimentation FFF work, scanning electron microscopy (SEM) was used to monitor the state of aggregation of the PMMA particles. Fractions of the PMMA sample were collected at predetermined elution volumes from the sedimentation FFF run. The fractions were then vacuum filtered onto 0.1 μm pore size Nuclepore filters (Pleasanton, CA, U.S.A.). The sample collected on the filter was then mounted on a standard SEM stub, gold coated with either a Technics Hummer III sputter coater (Alexandria, VA, U.S.A.) or a Vanton Vacuum Model Desk-I sputter coater (Cherry Hill, NJ, U.S.A.) and then observed either under a JEOL JSM35 scanning electron microscope (Tokyo, Japan) or a Hitachi S-450 scanning electron microscope (Tokyo, Japan).

RESULTS AND DISCUSSION

Representative fractograms of the two PMMA samples are shown in Fig. 1. These fractograms were obtained from sedimentation FFF system II with a carrier flow-rate of 0.80 ± 0.01 ml/min and a field strength of 61.6 *g*. The electron micrographs of these two PMMA samples are shown in Fig. 2. These micrographs show that the particle diameter is uniform whereas each fractogram in Fig. 1 displays a series of peaks that normally implies a non-uniformity in particle diameter. The logical explanation is that the first peak to elute represents (as we shall soon confirm) single latex particles. The second peak represents doublet particles, the third peak triplet clusters, and so on. Consistent with this explanation, clusters of various sizes are observed in the micrographs. The fractograms support the view that these are long-lived stable clusters rather than transient clusters formed during filtration for SEM sample analysis.

The resolution displayed in Fig. 1b is clearly better than that shown in Fig. 1a. Specifically, resolution values between singlet and doublet peaks are 1.43 and 1.20 for fractograms in Fig. 1a and b, respectively. The values which correspond to doublet and triplet peaks are 1.41 and 1.07. These differences in resolution can be attributed to the different polydispersities of the two samples of latex spheres. By combining the theory of band broadening and appropriate band-width measurements, the relevant polydispersities of the latex spheres can be ascertained.

Eqn. 10 shows that the polydispersity contribution to plate height H_p can be obtained as the intercept of a plot of plate height H *versus* flow velocity $<v>$. When data for the two single particle peaks studied here are plotted in this way, they yield straight lines as indicated in Fig. 3. The intercepts of the two lines differ substantially, indicating considerable differences in the two polydispersities.

Using the measured intercepts in conjunction with eqn. 12, the polydispersity (coefficient of variation) of the 0.207-μm latex spheres of Fig. 1a was found to be $(\sigma_d/d) = 0.040 \pm 0.012$, somewhat larger than the value $(\sigma_d/d) = 0.023 \pm 0.009$ determined for the 0.230-μm sample displayed in Fig. 1b. These results confirm that the fractograms of the respective PMMA samples shown in Fig. 1 differ in the resolution displayed primarily because of the differences in σ_d/d. Finite σ_d/d values not only interfere with apparent (not real) resolution but they put a limit on the maximum number of peaks that can be resolved.

Another important aspect of FFF theory is that the mean particle diameter d of a peak can be measured in terms of experimental retention volumes. This capability can be applied to the peaks in Fig. 1 to verify the assumed mechanism involving the aggregation of single particles. If the retention volumes of the first (singlet) peaks in Fig. 1 are measured and used in conjunction with eqns. 1, 4, and 5, the calculated particle diameters (using the reported densities of 1.21 g/ml) are 0.200 and 0.216 μm for Fig. 1a and b, respectively. These values are in good agreement with the reported diameters, 0.207 and 0.230 μm, respectively, and support the view that these peaks are composed of single latex beads.

We note that electron microscopy yields particle diameters of 0.200 ± 0.013 μm (measuring 133 particles) and 0.213 ± 0.013 μm (135 particles), respectively. The SEM calibration was performed using NBS standard SRM 1960 (9.89 μm) polystyrene beads[21].

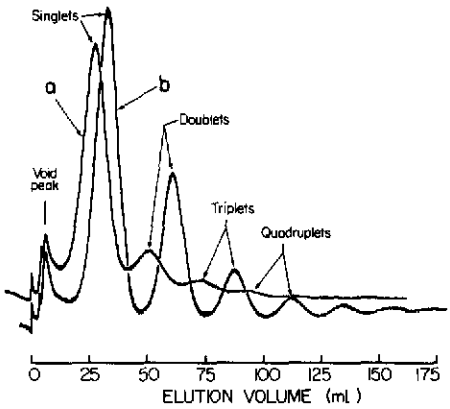

Fig. 1. Representative fractograms of aggregated PMMA latex samples obtained by system II at 61.6 *g* and a flow-rate of 0.80 ± 0.01 ml/min: (a) 0.207 μm PMMA aggregate series; (b) 0.230 μm PMMA aggregate series. Both samples were sonicated for about 30 min prior to runs.

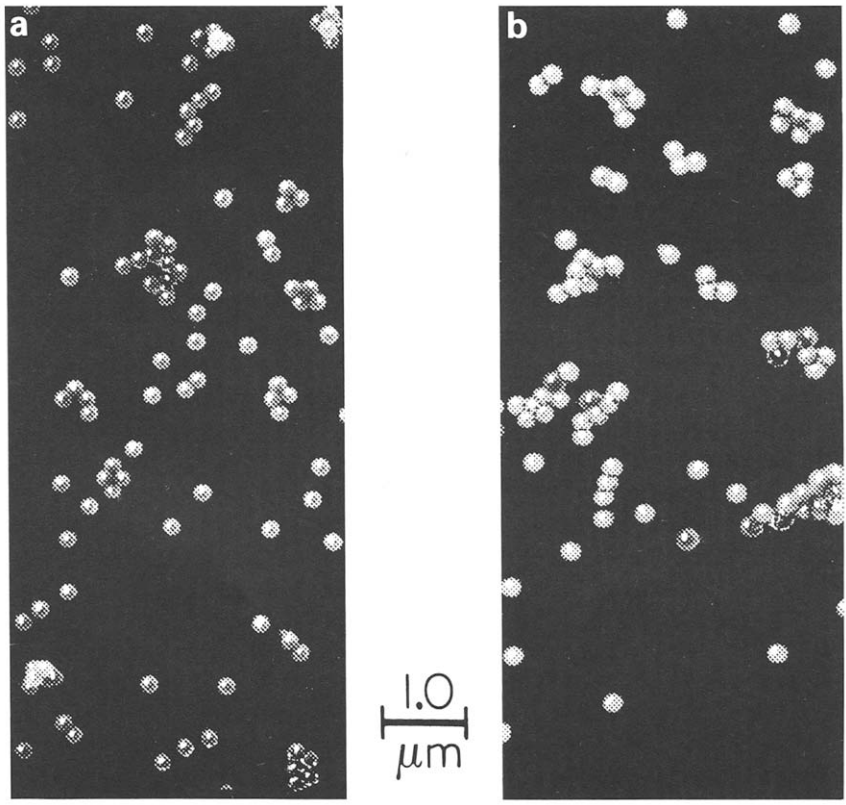

Fig. 2. Electron micrographs of (a) 0.207 μm and (b) 0.230 μm PMMA samples used to obtain fractograms in Figs. 1a and b, respectively.

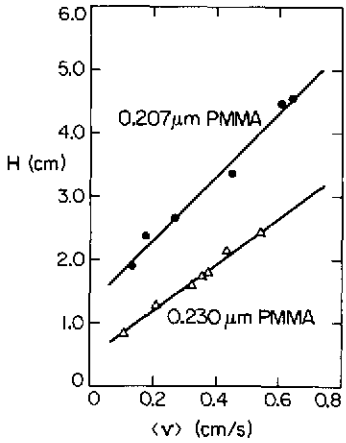

Fig. 3. Plate height H *versus* flow velocity $<v>$ plots for the singlet peaks of the two PMMA samples. Fractograms for plate height data were generated from system II at 61.6 *g*. Straight lines represent least squares fits: (a) 0.207 μm PMMA, $H = 1.30\ (\pm 0.12) + 5.01\ (\pm 0.29)\ <v>$; (b) 0.230 μm PMMA, $H = 0.435\ (\pm 0.065) + 3.364\ (\pm 0.057)\ <v>$.

The combination of eqns. 2, 3, and 5 shows that retention volume V_R is approximately proportional to particle mass. Thus singlets, doublets, triplets, and so on should appear as evenly spaced peaks along the elution volume axis. Fig. 1 is largely consistent with this conclusion but shows that the increment in V_R between successive peaks gradually falls off as V_R increases. Specifically, the retention volumes which correspond to the four successive peaks in Fig. 1a are 26.6, 51.4, 70.0 and 98.4 ml. Retention volumes for the six successive peaks of Fig. 1b are 32.9, 60.8, 87.7, 111.9, 134.2 and 155.2 ml.

Although the above calculations are highly supportive of the view that the peaks in Fig. 1 correspond to singlets, doublets, and higher order aggregates of the basic PMMA latex bead, a more absolute form of verification was obtained using electron microscopy. For this purpose narrow fractions or cuts were collected from the first five peaks of the nominal 0.207-μm PMMA sample at positions shown in Fig. 4. A fraction was also collected for the peak which appeared after the field was turned off. The individual fractions were then subjected to electron microscopy as described in the Experimental section. As expected, cut No. 1 yielded singlets, cut No. 2 yielded doublets, and so on. These results are shown in the electron micrographs displayed in Fig. 4.

Narrow fractions were also collected from the first six peaks of the 0.230-μm PMMA samples at positions shown in Fig. 5. We note that the difference in the two fractograms of 0.230 μm PMMA latex shown in Figs. 1b (system II) and 5 (system I) is due to the fact that Fig. 1b was obtained with a sonicated sample and Fig. 5 was obtained with the original sample. In the latter case the relative amount of higher order aggregated material is expected (and observed) to be high. The scanning electron micrographs of the fractions of the 0.230-μm sample indicated in Fig. 5 are shown in Fig. 6. The micrographs in Figs. 4 and 6 show that the resolution of different aggregate

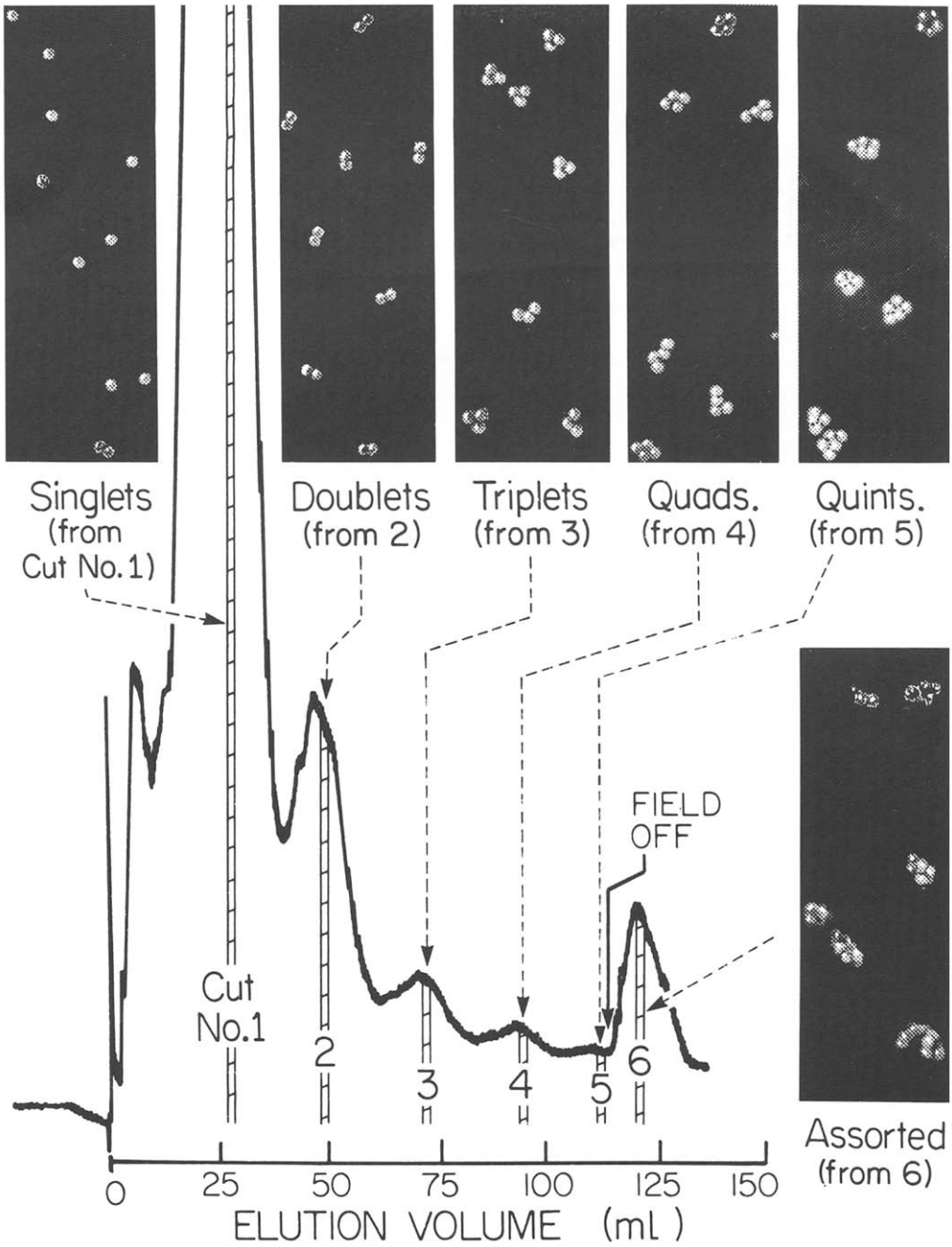

Fig. 4. Fractogram of 0.207 μm PMMA sample from which narrow fractions were cut. Inserted electron micrographs correspond to these fractions. Experimental conditions: sedimentation FFF system II was used at a field strength of 61.6 g and a flow-rate of 0.84 ml/min.

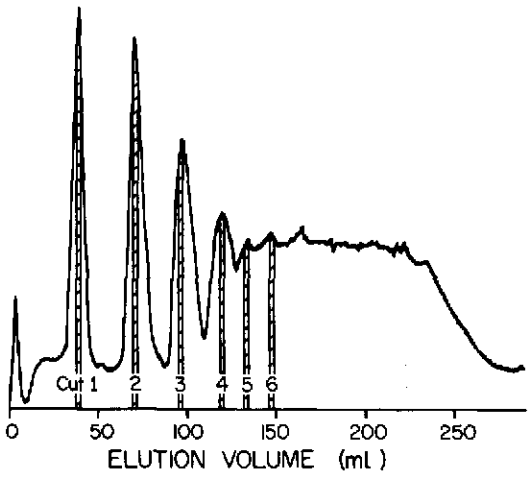

Fig. 5. Fractogram of 0.230 μm PMMA aggregate series from which six cuts were collected and prepared for SEM. Fractogram was obtained using system 1 and original sample. Experimental conditions: field strength 111 *g*, flow-rate 0.327 ml/min.

numbers is fairly complete, even for some cuts where the fractograms of Figs. 4 and 5 suggest incomplete resolution.

The micrographs in Figs. 4 and 6 show that the higher order PMMA aggregates vary considerably in shape. The assorted shapes co-elute in the same fraction but the different aggregation numbers do not, an observation confirming the theoretical conclusion (eqn. 3) that retention depends primarily on particle mass and density and not on shape.

Eqns. 10 and 11 show that sharper peaks and better resolution can be achieved by lowering the carrier liquid flow-rates in sedimentation FFF. This is consistent with previous observations[22]. Fig. 7, obtained using system I, shows the expected degradation of particle resolution with increasing flow-rate. A plot of R_s *versus* the relative mass difference $\Delta m/m$ for the singlet and doublet pair of peaks, the singlet and triplet pair, and the doublet and triplet peak pairs at the four flow-rates is shown in Fig. 8. This figure confirms the loss of resolution with increasing $<v>$. However, the resolution decrease is much less than predicted by the inverse $<v>^{1/2}$ dependence of eqn. 11 for $H_p = 0$, illustrating the important role played by polydispersity in peak resolution.

We note that the R_s values of Fig. 8 deviate from the linear dependence on $\Delta m/m$ suggested by eqn. 9. Closer analysis shows that strict linearity is not expected because of variations in N from one peak to another and the relatively large values of $\Delta m/m$.

The resolution of singlet/doublet PMMA particles illustrates the flexibility of sedimentation FFF in resolving aggregated from non-aggregated particles. Fig. 8 shows that an experimental field strength of 111 *g* (800 rpm) and a flow-rate of 0.327 ml/min yields $R_s = 2.38$, a value higher than needed. One can still achieve $R_s \approx 1.5$ for this pair at a flow-rate as high as 2.19 ml/min, this higher flow-rate increasing the speed of separation about seven-fold, down to *ca.* 30 min for elution of the doublet.

The average retention volume obtained for the first peak of each of the four

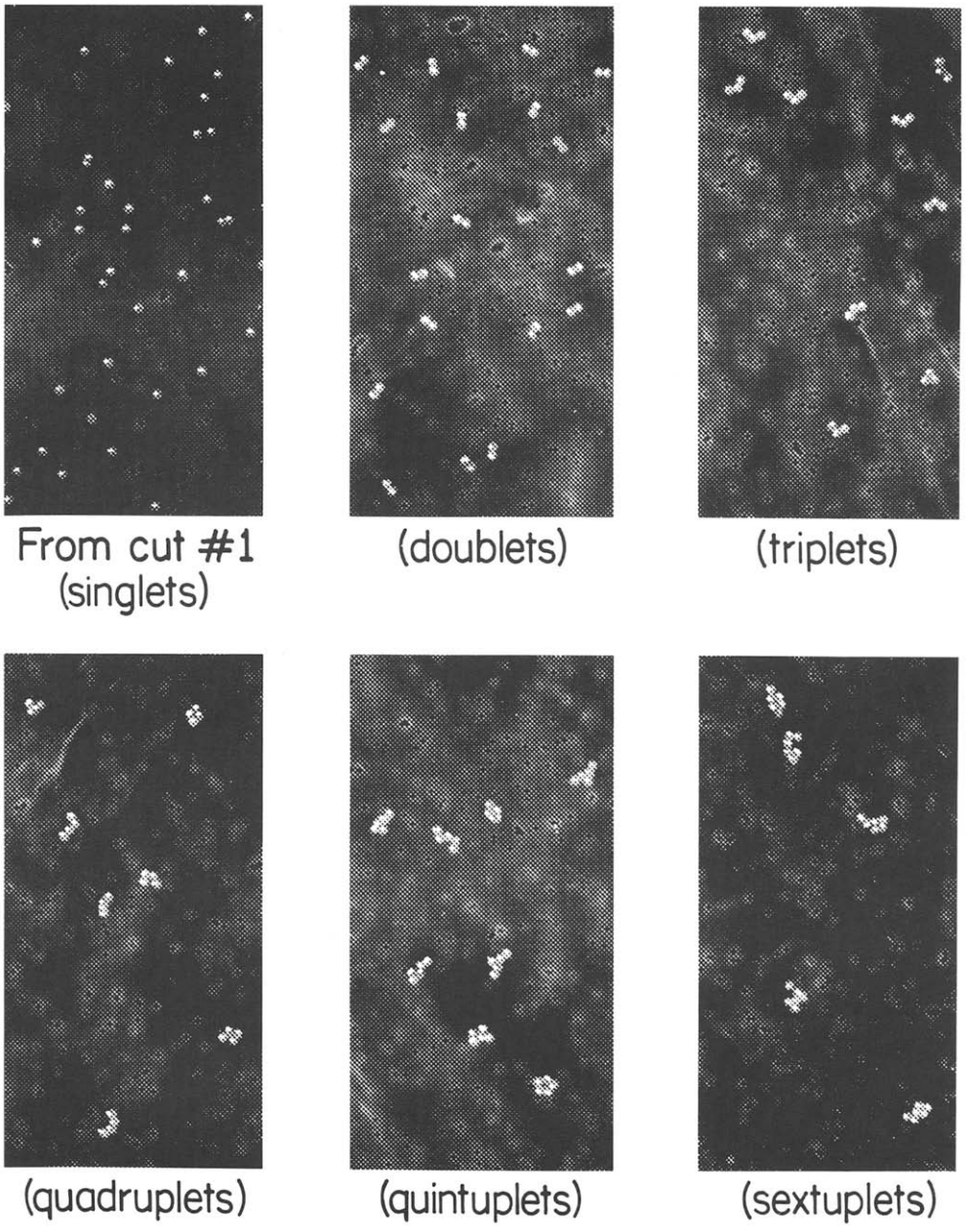

Fig. 6. Electron micrographs of cuts from the fractogram shown in Fig. 5.

fractograms in Fig. 7 is 40.2 $\pm$ 0.3 ml. This corresponds to a particle diameter of 0.213 μm, in excellent agreement with the value of 0.216 μm obtained for the first peak shown in the fractogram of Fig. 1b and also with the 0.213 μm value determined by SEM. The

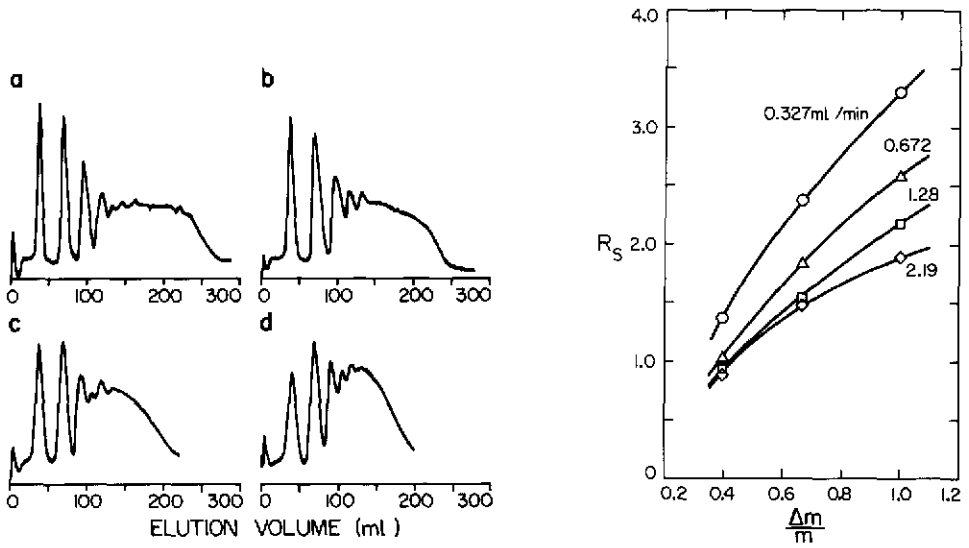

Fig. 7. Fractograms of 0.230 μm PMMA aggregate series obtained at 111.0 g using system I. The experimental flow-rates were varied as follows: (a) 0.327 ml/min, (b) 0.672 ml/min, (c) 1.28 ml/min, and (d) 2.19 ml/min.

Fig. 8. Plots of resolution, R_s, *versus* relative mass difference, $\Delta m/m$, at four different flow-rates (as indicated) for three pairs of peaks from the fractograms shown in Fig. 7. ($\Delta m/m$ = 0.4 for doublet-triplet pair, 0.667 for singlet-doublet pair, and unity for singlet-triplet pair.)

close agreement in these results is noteworthy considering that two different sedimentation FFF systems were used under different experimental conditions.

A close inspection of the fractograms in Figs. 5 and 7 shows that there are some measurable departures from the predictions of eqns. 1–4 for the aggregated particles. As noted previously, the spacing between successive peaks in both of the figures decreases as one proceeds along the elution scale. In contrast, eqns. 2 and 3 predict a constant interval between peaks. Compounding this anomaly is the observation from Fig. 7 that the spacing between successive peaks (and thus the position of all peaks past the singlet) depends upon the flow-rate, again in contradiction to the theoretical equations.

The major features of these anomalies can be explained in terms of the steric effect. Thus if we combine eqns. 3, 5, and 6 we find that retention volume V_R is described by the following relationship

$$V_R = \frac{Bm}{1 + A\gamma md} \tag{13}$$

where A and B are constants. The term in the denominator containing A is the steric term which derives from the first term on the right of eqn. 6. If the steric term were negligible, A, for all practical purposes, would equal zero. In this limiting case the retention volume is predicted to increase in direct proportion to mass and therefore in

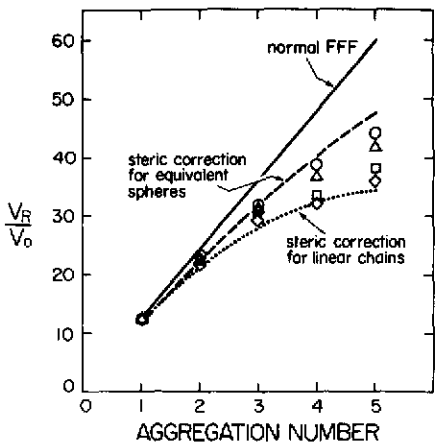

Fig. 9. Plot of V_R/V_0 *versus* aggregation number showing several theoretical lines. The upper line assumes normal FFF; the middle and lower lines incorporate steric corrections for spherical and straight chains geometries, respectively. (○) Flow-rate = 0.327 ml/min; (△) flow-rate = 0.672 ml/min; (□) flow-rate = 1.28 ml/min; (◇) flow-rate = 2.19 ml/min. Experimental points are obtained from fractograms given in Fig. 7.

direct proportion to aggregation number, which would lead to even spacing between all peaks. However, the A-containing term, which grows in proportion to both particle mass m and effective diameter d, increasingly erodes the ideal retention volume $V_R = Bm$ as particle size increases. Therefore the interval between successive peaks decreases as the aggregation number increases in conformity with experimental observations.

With regard to the velocity dependence of the peak spacing, we have known for some time that hydrodynamic lift forces serve to modulate the steric effect[23]. The practical consequence of this important factor is that parameter γ (which reflects lift force effects) increases with flow velocity $<v>$. Thus the steric term in eqn. 13 is increasingly magnified in effect as the flow velocity increases, leading to a velocity-dependent spacing between higher-order peaks as clearly observed in Fig. 7.

The velocity dependence of γ not only influences the distinguishable peaks of Fig. 7 but it also serves to shift the featureless signal on the right side of the fractograms, corresponding to the larger aggregates, to lower retention volumes with increasing flow-rate. It is very likely that the rather sudden dropoff of the signal on the far righthand side of the fractograms represents the steric transition or inversion point where steric FFF gains dominance over normal FFF[15].

The steric influence is further clarified in Fig. 9 which shows a plot of the ratio of retention volume V_R to void volume V_0 against the aggregation number. Along with the experimental data obtained at the various flow-rates, three theoretical curves (based on $d = 0.213$ μm) are shown. The upper curve corresponds to the operation of normal FFF without the intervention of the steric effect. The middle curve accounts for the steric effect under the assumption that $\gamma = 1$ and that the aggregate particles effectively coalesce into a spherical particle. The bottom curve is also based on the assumption that $\gamma = 1$, but the effective diameter d used in the steric term was given

a value at the opposite extreme, corresponding to the full length of a linear array of the aggregated latex spheres. We observe that the experimental points lie at some intermediate position between the bottom and middle line. The electron micrographs of Figs. 4 and 6 confirm that the aggregate clusters tend to be somewhat extended in space with little indication that the most compact cluster geometry is generally favored. Thus it is not surprising to see the experimental results drop well below the middle line of Fig. 9. However, since few of the observed clusters are maximally extended in a linear array geometry, the results would not be expected to approach the bottom curve of Fig. 9. Thus the intermediate range between these curves is consistent with expectation.

We note that steric effects, even for perfect spheres, are not yet subject to exact calculation; for geometrically complex bodies such as latex aggregates the magnitude of steric effects can only be predicted with considerable guesswork. Experiments of the kind reported here should eventually clarify the magnitude of such steric effects under diverse conditions.

CONCLUSIONS

The above study demonstrates that successive aggregates of small colloidal particles can be isolated from one another providing the particle size distribution is sufficiently narrow. Furthermore, the breadth of this distribution (the polydispersity) can be obtained using plots of plate height *versus* flow velocity. The conditions for such studies can be optimized on the basis of theory.

While all sedimentation FFF results are subject to some steric perturbations as particle size and mass increase, this effect is particularly severe in the present case because the particle aggregates assume rather extended structures of relatively large dimensions which serve to enhance the steric effect. Since it takes a linear array of only four of the 0.230-μm PMMA latex beads to generate a particle almost 1 μm in length, many of the larger clusters with aggregation numbers of 4, 5, 6, and beyond will have particles in this size range. Particles this large have long been known to have significant steric effects. These effects increase with flow velocity. We conclude that such steric effects must not only be accounted for in studies of particle aggregation but also in the study of other open dendritic type structures where the effective diameter is amplified out of proportion to the particle mass involved. A small amount of steric perturbation is observed even for the dimer particles (as reflected in the reduced peak spacing) which are less than 0.5 μm in length. We have observed steric perturbations under some conditions for spheres down to *ca.* 0.35 μm. It is likely that the steric effect is also responsible for the velocity-dependent anomalies observed by Kirkland *et al.*[10] in the study of needlelike and platelike particles whose longest dimensions were *ca.* 1 μm.

ACKNOWLEDGEMENT

This work was supported by grant DE-FG02-86ER60431 from the Department of Energy.

REFERENCES

1 J. C. Giddings, G. Karaiskakis, K. D. Caldwell and M. N. Myers, *J. Colloid Interface Sci.*, 92 (1983) 66.
2 J. C. Giddings, *Sep. Sci. Technol.*, 19 (1984) 831.
3 J. C. Giddings, K. D. Caldwell and H. K. Jones, in T. Provder (Editor), *Particle Size Distribution: Assessment and Characterization*, ACS Symposium Series No. 332, 1987, Ch. 15.
4 M. D. Summers and G. E. Smith, *Virology*, 84 (1978) 390.
5 F. Family and D. P. Landau (Editors), *Kinetics of Aggregation and Gelation*, North Holland, Amsterdam, 1984.
6 K. D. Caldwell, T. T. Nguyen, J. C. Giddings and H. M. Mazzone, *J. Virol. Methods*, 1 (1980) 241.
7 J. C. Giddings, F. J. F. Yang and M. N. Myers, *Anal. Chem.*, 46 (1974) 1917.
8 F. J. F. Yang, M. N. Myers and J. C. Giddings, *Anal. Chem.*, 46 (1974) 1924.
9 F. J. Yang, M. N. Myers and J. C. Giddings, *J. Colloid Interface Sci.*, 60 (1977) 574.
10 J. J. Kirkland, L. E. Schallinger and W. W. Yau, *Anal. Chem.*, 57 (1985) 2271.
11 J. Janca, D. Pribylova, K. Bouchal, V. Tyrackova and E. Zurkova, *J. Liq. Chromatogr.*, 9 (1986) 2059.
12 J. C. Giddings and M. N. Myers, *Sep. Sci. Technol.*, 13 (1978) 637.
13 H. Small, *J. Colloid Interface Sci.*, 48 (1974) 147.
14 M. N. Myers and J. C. Giddings, *Anal. Chem.*, 54 (1982) 2284.
15 S. Lee and J. C. Giddings, *Anal. Chem.*, in press.
16 T. Koch and J. C. Giddings, *Anal. Chem.*, 58 (1986) 994.
17 J. C. Giddings, *Dynamics of Chromatography: Part I, Principles and Theory*, Dekker, New York, 1965.
18 J. C. Giddings, *Pure Appl. Chem.*, 51 (1979) 1459.
19 H. K. Jones, K. Phelan, M. N. Myers and J. C. Giddings, *J. Colloid Interface Sci.*, 120 (1987) 140.
20 J. C. Giddings, *Anal. Chem.*, 57 (1985) 945.
21 S. Ratanathanawongs, private communication.
22 G. Karaiskakis, M. N. Myers, K. D. Caldwell and J. C. Giddings, *Anal. Chem.*, 53 (1981) 1314.
23 K. D. Caldwell, T. T. Nguyen, M. N. Myers and J. C. Giddings, *Sep. Sci. Technol.*, 14 (1979) 935.